Global and Planetary Change 146 (2016) 30–37

Contents lists available at ScienceDirect

Global and Planetary Change

journal homepage: www.elsevier.com/locate/gloplacha

CMIP5 downscaling and its uncertainty in China

TianXiang Yue [a,*], Na Zhao [a], ZeMeng Fan [a,*], Jing Li [a], ChuanFa Chen [b], YiMin Lu [c], ChenLiang Wang [a], Bing Xu [d], John Wilson [a,e]

[a] State Key Laboratory of Resources and Environment Information System, Institute of Geograpical Science and Natural Resources Research, Chinese Academy of Sciences, 11A, Datun Road, Anwai, 100101 Beijing, China
[b] Geomatics College, Shandong University of Science and Technology, 266510 Qingdao, Shandong Province, China
[c] Key Lab of Spatial Data Mining and Information Sharing, Fuzhou University, No. 523, Gongye Road, 350002 Fuzhou, China
[d] Center for Earth System Science, Tsinghua University, 100084 Beijing, China
[e] Spatial Sciences Institute, Dana and David Dornsife College of Letters, Arts and Sciences, University of Southern California, United States

ARTICLE INFO

Article history:
Received 10 December 2015
Received in revised form 9 September 2016
Accepted 14 September 2016
Available online 15 September 2016

Keywords:
Spatial stationarity, non-stationarity
HASM-OLS
HASM-GB
Climate scenarios
Downscaling
Uncertainty

ABSTRACT

A comparison between the Coupled Model Intercomparison Project Phase 5 (CMIP5) data and observations at 735 meteorological stations indicated that mean annual temperature (MAT) was underestimated about 1.8 °C while mean annual precipitation (MAP) was overestimated about 263 mm in general across the whole of China. A statistical analysis of China-CMIP5 data demonstrated that MAT exhibits spatial stationarity, while MAP exhibits spatial non-stationarity. MAT and MAP data from the China-CMIP5 dataset were downscaled by combining statistical approaches with a method for high accuracy surface modeling (HASM). A statistical transfer function (STF) of MAT was formulated using minimized residuals output by HASM with an ordinary least squares (OLS) linear equation that used latitude and elevation as independent variables, abbreviated as HASM-OLS. The STF of MAP under a BOX-COX transformation was derived as a combination of minimized residuals output by HASM with a geographically weight regression (GWR) using latitude, longitude, elevation and impact coefficient of aspect as independent variables, abbreviated as HASM-GB. Cross validation, using observational data from the 735 meteorological stations across China for the period 1976 to 2005, indicates that the largest uncertainty occurred on the Tibet plateau with mean absolute errors (MAEs) of MAT and MAP as high as 4.64 °C and 770.51 mm, respectively. The downscaling processes of HASM-OLS and HASM-GB generated MAEs of MAT and MAP that were 67.16% and 77.43% lower, respectively across the whole of China on average, and 88.48% and 97.09% lower for the Tibet plateau.

1. Introduction

GCMs are an available source for climate scenarios. However, due to the coarse spatial resolution of GCMs (200–500 km), it is difficult to assess climate change impacts at regional and local levels, although GCMs can provide a good overview of both current and future climates at a global level (Xue et al., 2007). Grotch and MacCracken (1991) found that the range of changes in temperature and precipitation simulated by different models is much broader at finer spatial scales. von Storch et al. (1993) observed that simulations of GCMs were questionable on a regional level. Ciret and Sellers (1998) stated that increasing the spatial resolution of GCMs would improve the simulation of climate and hence increase confidence in the use of GCM output for impact studies. Raisanen (2007) concluded that many small-scale processes could not be simulated explicitly in GCMs. Prudhomme and Davies (2009) indicated that different GCMs often resulted in different climate outputs from the same atmospheric and oceanic drivers, especially at regional scales.

The CMIP5 models may not well simulate different kinds of precipitation over eastern China, while the higher resolution version better represents the frequency distribution of precipitation (Huang et al., 2013). The CMIP5 models simulated the seasonal mean and variability of summer rainfall reasonably well but failed to resolve extremes, the diurnal cycle, and the dynamic forcing of precipitation; downscaling to 30 km improved these characteristics of precipitation, with the greatest improvement in the representation of extremes in the central U.S. (Harding et al., 2013).

Many dynamic downscaling methods (DDMs) and statistical downscaling approaches (SDAs) have been developed to improve the poor performance of GCMs at local and regional scales. DDMs are based on Regional Climate Models (RCMs) or Limited Area Models (LAMs) that have finer horizontal grid resolution of surface features (Xu, 1999; Laprise, 2008). For instance, a fine computational grid over a limited domain was nested within the coarse grid of a GCM in LAMs (Anthes, 1983; Giorgi, 1990; Walsh and McGregor, 1997). A numerical method

* Corresponding authors.
E-mail addresses: Yue@lreis.ac.cn (T. Yue), fanzm@lreis.ac.cn (Z. Fan).

http://dx.doi.org/10.1016/j.gloplacha.2016.09.003
0921-8181/

for modeling climate on a regional scale was developed, whereby large-scale weather systems were simulated with a GCM and the GCM output was used to provide boundary conditions needed for high-resolution mesoscale model simulations over the region of interest (Dickinson et al., 1989). A one-way nesting method was used to develop a regional climate model (RCM) on a spatial resolution of 50 km × 50 km driven by the output from a GCM (Jones et al., 1995). A RCM, the non-hydrostatic Weather Research and Forecasting model (WRF), was nested into the climate forecast system (CFS) of the coupled atmosphere-ocean general circulation model (CGCM) from the National Center for Environmental Prediction (NCEP) to downscale the winter precipitation prediction over continental China between 1982 and 2008. A comparison of DDMs and SDAs indicated that a DDM based on non-linear artificial neural networks was found to be the best at modeling the inter-annual variability of rainfall indices (Haylock et al., 2006). The optimized WRF reduced error from the optimized CFS by 30% and increased pattern correlation by 0.12 (Yuan et al., 2012). It was found that the majority of the difference in precipitation between the RCM and GCM can be explained by their difference in topographic height (Tselioudis et al., 2012). These DDMs have many disadvantages such as their extensive and costly computing requirements, too coarse resolutions (in the order of 11 km) that are not suitable for local scale studies, their dependence on lateral and lower boundary conditions prescribed by the GCM, and assumptions of stationarity incorporated within their many sub-grid parameterization schemes (Khalili et al., 2013).

The derivation of local scale information from integrations of coarse-resolution GCMs with the help of statistical models fitted to present observations is generally referred to as SDA (Zorita and von Storch, 1999). SDAs uses statistical transfer functions (STFs) representing observed relationships between larger-scale atmospheric variables and local quantities (Pielke and Wilby, 2012). Statistical approaches have been widely used to bridge the gap between the large- and the local-scale (e.g., Hewitson and Crane, 1996; Charles et al., 1999; Wilby et al., 2002; Gachon and Dibike, 2007; Dibike et al., 2008).

Downscaling GCMs using STFs have emerged as a popular approach to increase spatial resolutions and therefore makes GCMs more applicable to regional and local analysis in China. For instance, an STF was evaluated with daily mean air temperature, pan-evaporation, and precipitation data (1961–2000) from 11 weather stations in the Haihe River basin; the results showed that the coefficients of determination between observed and downscaled mean temperature, pan-evaporation, and precipitation were 99%, 93%, and 73%, respectively (Chu et al., 2010). An STF was applied to generate a daily time-series of temperature and precipitation (1961–2099) estimates for the Yellow River Basin using outputs from the third version of the Hadley Center coupled model (HadCM3); the projections showed that annual average maximum and minimum temperature would rise by 5.0 °C and annual precipitation would increase by 54–150 mm in the 2080s (Liu et al., 2011a). Two STFs, the nonhomogeneous hidden Markov model (NHMM) and the statistical down-scaling model (SDSM), were evaluated based on observed daily precipitation over the Tarim River basin, an arid basin in western China; results showed that there was little difference in model performance for dry- and wet-spell length between NHMM and SDSM, but NHMM exhibited better performance than SDSM for wet-day precipitation estimates (Liu et al., 2011b). An STF was presented on the basis of the relationships between precipitation and other environmental factors in the Qaidam Basin such as topography and vegetation, which was developed for downscaling the spatial precipitation fields of these remote sensing products (Jia et al., 2011).

An STF was built up to construct future scenarios of extreme daily temperature, and precipitation in the Dongjiang River basin of China in the 21st century from the HadCM3 model under the A2 and B2 emission scenarios; the biases for the maximum temperature, minimum temperature, and precipitation were 1.1 °C, 0.12 °C, and 0.39 mm/day (Yang et al., 2012). An STF was used to spatially downscale extreme precipitation and temperature indices of six GCMs under three emission scenarios (A1B, A2, B1) from grid outputs to target stations to project their potential spatio-temporal changes on the Loess Plateau of China during the 21st century. The results indicated that the present change trend of extreme climate would continue during the 21st century, i.e. longer heat-wave duration and growing season length, less cold extremes, smaller annual extreme temperature range, more frequent and intense precipitation, and longer drought duration (Li et al., 2012). An STF based on GCM outputs from a project of the Development of a European Multi-model Ensemble System for Seasonal to Interannual Prediction (DEMETER) and observation data of large-scale circulation variables was used to predict autumn precipitation in China (Liu and Fan, 2013).

In this article, STFs for mean annual temperature (MAT) and mean annual precipitation (MAP) are developed by analyzing spatial stationarity. The STFs are constructed by a combination of trend surfaces with a method for high accuracy surface modeling (HASM) (Yue, 2011; Yue et al., 2013b).

2. Materials and methods

The CMIP5 datasets of monthly mean temperature and precipitation were provided by the National Climate Center of China. They include historical simulations and three Representative Concentration Pathway (RCP) scenarios, RCP2.6, RCP4.5 and RCP8.5. They were created by using the simple average of the outputs from the 21 CMIP5 models for which the spatial resolutions are unified into 1° × 1° by ANUSPLIN interpolation.

Ten-day observation data of temperature and precipitation were collected from 735 meteorological stations scattered across China from 1961 to 2010 (National Meteorological Information Center of China: http://www.nmic.gov.cn) (Fig. 1a). A digital elevation model (DEM) from the Shuttle Radar Topography Mission (SRTM) of China at a spatial resolution of 90 × 90 m (http://srtm.csi.cgiar.org) was upscaled into a DEM at a spatial resolution of 1 km × 1 km using a cubic convolution resampling approach. The DEM was used as auxiliary data to develop the statistical transfer function for MAT and MAP.

A zoning system dividing the land mass of China into nine regions in terms of matching temperature, precipitation and soil was adopted to make it easier to analyze the changes in precipitation and temperature from one place to another (Zhou et al., 1981). The nine regions are respectively termed as Ri, i = 1, 2, … ,9 (Fig. 1b).

A rectangular region (60°E–149°E, 0.5°N–49.5°N) was extracted from the CMIP5 datasets, which covers the whole land mass of China. It is termed a China-CMIP5 dataset. It includes 90 × 50 = 4500 grid cells.

A variation coefficient can be formulated as:

$$CV = \frac{\sigma}{\overline{Z}} \times 100\% \quad (1)$$

where σ is the standard deviation and $\overline{Z}$ represents a mean property value.

Latitude and elevation were selected as explanatory variables for simulating MAT by means of geographically weighted regression (GWR). Then, we obtained three surfaces representing the intercept, latitude regression coefficient and elevation regression coefficient. The variation coefficients of the intercept, latitude regression coefficient and elevation regression coefficient were 24.66%, 23.36% and 21.30%, respectively, measured in terms of the variation coefficient formulation. They are all less than 25%. This means that MAT exhibits spatial stationarity and that trend surfaces of MAT can be simulated by ordinary least squares (OLS).

The OLS equation of MAT using the China-CMIP5 dataset and taking the DEM at the spatial resolution of 1 km × 1 km as auxiliary data can be expressed:

$$RMAT(x, y) = 41.585 - 10^{-5} \cdot (0.982y - 404.090Ele(x, y)) \quad (2)$$

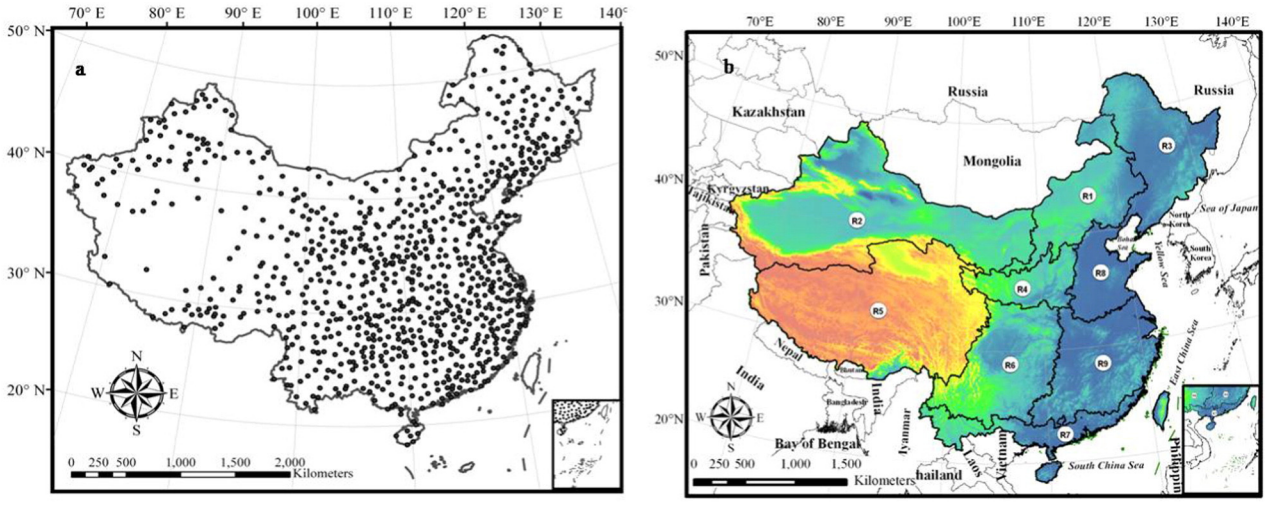

Fig. 1. Maps showing (a) the spatial distribution of the meteorological stations in China, and (b) a digital elevation model with the nine regions of China overlaid.

where $RMAT(x,y)$is MAT from the OLS regression of the China-CMIP5 data during the period from 1976 to 2005, y represents latitude (m), and $Ele(x,y)$ is the elevation (m) at the location (x,y).

The downscaling formulation of MAT can be expressed as:

$$DMAT(x,y) = RMAT(x,y) + HASM(MAT_j - RMAT_j) \tag{3}$$

where $DMAT(x,y)$represents the downscaled MAT, MAT_j the observed MAT at meteorological station j, $HASM(MAT_j - RMAT_j)$ the residual surfaces of the downscaled MAT improved by HASM at the spatial resolution of 1 km × 1 km (Yue, 2011; Yue et al., 2013a).

Surfaces of latitude, longitude, elevation and aspect regression coefficients as well as intercept can be created by simulating the relationship of MAP from the China-CMIP5 dataset with latitude, longitude, elevation and aspect using GWR. The variation coefficients of the surfaces of the longitude and aspect regression coefficients exceeded 100%, which indicates strong variation; those for the latitude and elevation regression coefficients as well as the intercept are greater than 40%, indicating moderate variability. Latitude, longitude, elevation and aspect as well as intercept are non-stationary at the 1% significance level. It is better to simulate MAP by means of GWR. In other words, MAT can be modeled as a linear function of latitude and elevation, while regression coefficients of latitude, longitude, elevation and aspect for MAP are best determined locally instead of globally.

MAP values from the China-CMIP5 dataset were normalized by using the following formulation to stabilize the simulation processes:

$$P(x,y) = \frac{OMAP(x,y)}{MAX\{OMAP(x,y)\}} \tag{4}$$

where $P(x,y)$ is a normalization value of MAP at grid cell (x,y) during the period from 1976 to 2005,$OMAP(x,y)$ is the original MAP from the China-CMIP5 dataset during the period from 1976 to 2005, and $MAX\{OMAP(x,y)\}$ is the maximum value of MAP from the China-CMIP5 dataset during the period.

To ensure the normality of GWR, a BOX-COX transformation of$P(x,y)$ (Box and Cox, 1964) was conducted as follows:

$$\Psi_{0.4}(P(x,y)) = \left((P(x,y))^{0.4} - 1\right)/0.4 \tag{5}$$

A trend surface of the transformed $P(x,y)$ was then created by means of GWR:

$$\Psi_{0.4}(P(xy)x) = \theta_0(xy) + \theta_1(xy)\cdot x + \theta_2(xy)\cdot y + \theta_3(xy)\cdot Ele(xy) + \theta_4(xy)\cdot ICA(xy) \tag{6}$$

where $\theta_1(x,y)$, $\theta_2(x,y)$, $\theta_3(x,y)$ and $\theta_4(x,y)$as well as $\theta_0(x,y)$are respectively the coefficients of the latitude, longitude, elevation, aspect, and the intercept.

The MAP observations from meteorological stations were employed to improve the trend surface. The normalized downscaled-OMAP with the BOX-COX transformation at a spatial resolution of 1 km × 1 km can be formulated as follows:

$$\begin{aligned}\Psi_{0.4}(dMAP(x,y)) &= \Psi_{0.4}(P(x,y)) + HASM\{\Psi_{0.4}(MAP_j/MAX\{MAP_j(x,y)\}) - \Psi_{0.4}(P(x,y)\}\\ &= \Psi_{0.4}(P(x,y)) + HASM\{\varepsilon_j\}\end{aligned} \tag{7}$$

where $\varepsilon_j = \Psi_{0.4}(MAP_j/MAX\{MAP_j(x,y)\}) - \Psi_{0.4}(P(x,y)$is the residue of $\Psi_{0.4}(P(x,y))$ at meteorological station j, $HASM\{\varepsilon_j\}$ represents the spatial interpolation of the residues at the meteorological stations, MAP_j is the observed MAP at meteorological station j, and $dMAP(x,y)$ is the normalized downscaled-OMAP at the location (x,y) during the period from 1976 to 2005.

After an inverse BOX-COX transformation and inverse normalization, the downscaled-OMAP was finally formulated as follows:

$$DMAP(x,y) = MAX\{OMAP(x,y)\}\cdot(0.4\cdot\Psi_{0.4}(dMAP(x,y)) + 1)^{\frac{1}{0.4}} \tag{8}$$

The procedure from Eqs. (4) to (8) is termed as HASM-GB. Similarly, we can get IDW-GB, OK-GB and Spline-GB when IDW, ordinary Kriging (OK) and Spline are used to interpolate the residues, respectively. The process of Eqs. (2) and (3) is termed HASM-OLS and IDW-OLS, OK-OLS and Spline-OLS could be developed in similar ways.

3. Validation

3.1. Comparison of accuracies from different approaches.

The mean absolute and mean relative errors of the downscaled OMAT and OMAP surfaces were formulated as follows:

$$DTAE = \frac{1}{n}\times\sum_{j=1}^{n}|DMAT_j\text{-}MAT_j| \tag{9}$$

$$DTRE = 100\%\times DTAE/\left(\frac{1}{n}\sum_{j=1}^{n}|MAT_j|\right) \tag{10}$$

$$DPAE = \frac{1}{n}\times\sum_{j=1}^{n}|DMAP_j\text{-}MAP_j| \tag{11}$$

Table 1
Comparison of accuracies of downscaled CMIP5 using different methods.

Error		IDW	Kriging	Spline	IDW-OLS	Kriging-OLS	Spline-OLS	HASM-OLS
MAT	DTAE (°C)	14.11	14.15	14.16	0.66	0.67	1.11	0.66
	DTRE (%)	128	128	128	6	6	10	5
MAP	DPAE (mm)	333	334	334	86	81	139	79
	DPRE (%)	42	42	42	11	10	17	9

$$DPRE = 100\% \times DPAE / \left(\frac{1}{n} \sum_{j=1}^{n} |MAP_j| \right) \quad (12)$$

where $DMAT_j$ and $DMAP_j$ are respectively the downscaled OMAT and OMAP at meteorological station j, MAT_j and MAP_j are respectively the observed MAT and MAP at meteorological station j, $DTAE$ and $DPAE$ are the mean absolute errors of the downscaled OMAT and OMAP, and $DTRE$ and $DPRE$ are the mean relative errors of the downscaled OMAT and OMAP.

The results from different methods indicated that consideration of non-stationarity can efficiently improve the accuracy of the simulated climatic elements (Table 1). The relative errors of the downscaled OMAT using IDW-OLS, Kriging-OLS and Spline-OLS were decreased by 122%, 122% and 118%, respectively compared with the ones using IDW, OK, and Spline. The relative errors of the downscaled OMAP generated with IDW-GB, Kriging-GB and Spline-GB were 31%, 32% and 25% lower, respectively than those generated with IDW, Kriging and Spline. The best results were obtained when HASM-OLS and HASM-GB were employed to downscale OMAT and OMAP since the absolute errors were 0.66 °C and 79 mm and the relative errors were 5% and 9%, respectively. HASM-OLS and HASM-GB were at least 1% more accurate than all of the improved classic methods.

3.2. Validation of CMIP5 baseline data

Regression analysis for the whole land mass of China produced correlation coefficients of $\{OMAT_j\}$ with $\{MAT_j\}$ and of $\{OMAP_j\}$ with $\{MAP_j\}$ of 0.90 and 0.82, respectively, while the ones for $\{DMAT_j\}$ with $\{MAT_j\}$ and $\{DMAP_j\}$ with $\{MAP_j\}$ were 0.99 and 0.97, respectively in which $OMAT_j$ and $OMAP_j$ represent respectively OMAT and OMAP at meteorological station j, MAT_j and MAP_j the observed MAT and MAP at meteorological station j, $DMAT_j$ and $DMAP_j$ the downscaled OMAT and OMAP at meteorological station j by means of HASM-OLS and HASM-GB respectively, $j = 1, 2, \ldots, 735$. In other words, the downscaling processes made the correlation coefficient of annual mean temperature 10% higher and that for mean annual precipitation 18% higher (Figs. 2 and 3).

Results from HASM-OLS and HASM-GB were cross-validated using observational data from meteorological stations across China for the period 1976–2005. Cross-validation was comprised of four steps: (1) 10% of the meteorological stations were removed for validation prior to model creation; (2) DMAT and DMAP during the period 1976–2005 were calculated at a spatial resolution of 1 km × 1 km using the remaining 90% of the meteorological stations; (3) MAE was calculated using the 10% removed meteorological stations; and (4) the 10% removed meteorological stations were then returned to the pool of available stations. This process is repeated until DMAT and DMAP at all meteorological stations have been validated in this manner and simulation error statistics were obtained.

We used six indices to formulate the MAEs of OMAT and OMAP as well as the reduction of the MAEs using the HASM-OLS and HASM-GB downscaling processes as follows:

$$OTAE(i) = \frac{1}{n_i} \times \sum_{j=1}^{n_i} |OMAT_j(i) - MAT_j(i)| \quad (13)$$

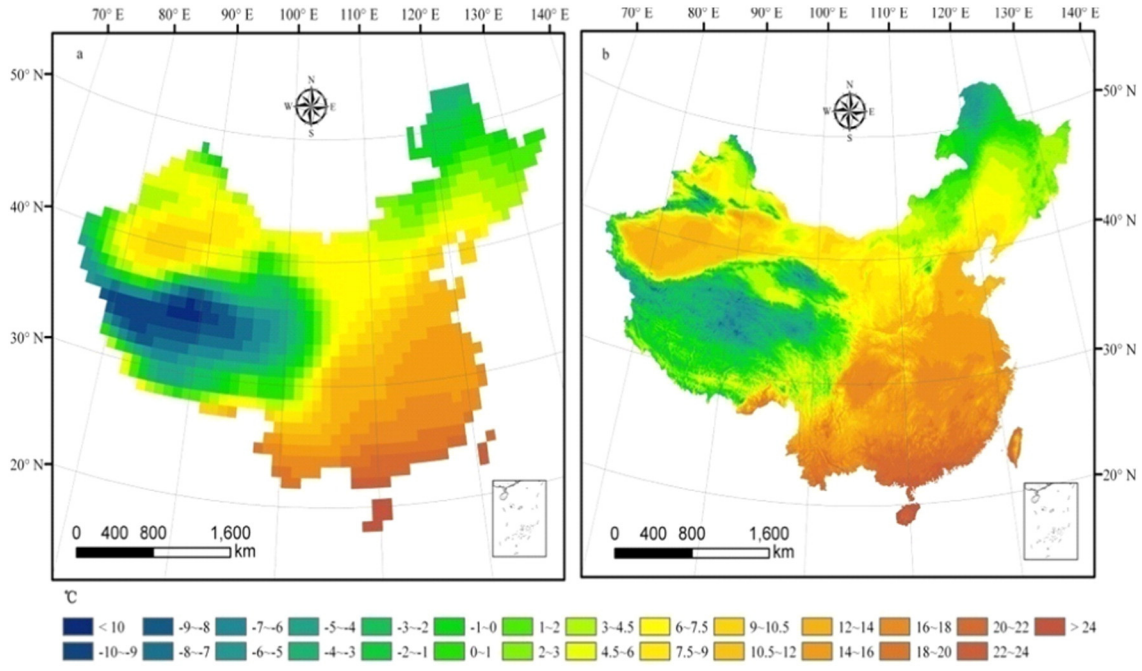

Fig. 2. Map showing (a) the OMAT from the China-CMIP5 dataset; and (b) the downscaled MAT.

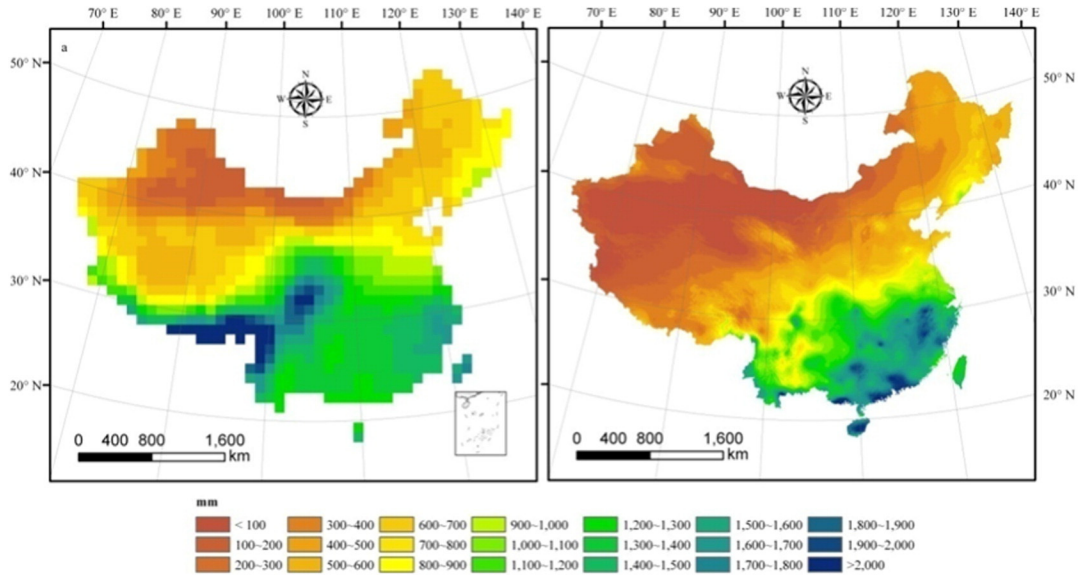

Fig. 3. Map showing (a) the OMAP from the China-CMIP5 dataset; and (b) the downscaled MAP.

$$OPAE(i) = \frac{1}{n_i} \times \sum_{j=1}^{n_i} \left| OMAP_j(i) - MAP_j(i) \right| \quad (14)$$

$$DTAE(i) = \frac{1}{n_i} \times \sum_{j=1}^{n_i} \left| DMAT_j(i) - MAT_j(i) \right| \quad (15)$$

$$DPAE(i) = \frac{1}{n_i} \times \sum_{j=1}^{n_i} \left| DMAP_j(i) - MAP_j(i) \right| \quad (16)$$

$$RT(i) = 100\% \times (OTAE(i) - DTAE(i))/OTAE(i) \quad (17)$$

$$RP(i) = 100\% \times (OPAE(i) - DPAE(i))/OPAE(i) \quad (18)$$

where $i = 1, 2, \ldots, 8$ and 9 represent respectively regions R_1, R_2, …, R_8 and R_9; n_i is the total number of meteorological stations in region R_i; *OTAE* and *OPAE* are respectively the MAEs of OMAT and OMAP; *DTAE* and *DPAE* are respectively the MAE of the downscaled MAT and MAP; *RT* and *RP* respectively represent the improved ratios of the MAEs by the downscaling processes of OMAT and OMAP; $OMAT_j(i)$ and $OMAP_j(i)$ are respectively the original MAT and MAP from the China-CMIP5 dataset at the *j*th meteorological station in the region R_i; $DMAT_j(i)$ and $DMAP_j(i)$ are respectively the downscaled MAT and MAP at the *j*th meteorological station in the region R_i; and $MAT_j(i)$ and $MAP_j(i)$ are respectively observed MAT and MAP at the *j*th meteorological station in the region R_i.

Validation results indicated that the MAE of OMAT was 2.04 °C for the whole of China on average (Table 2). The regions, which had larger MAEs than the whole of China, included the regions R_5 (Tibet plateau), R_2 (arid area), R_4 (Loess plateau), and R_6 (Sichuan Basin plus Yunnan-Guizhou plateau). Their MAEs were respectively 4.64, 3.39, 2.58 and 2.64 °C because the OMAT from the China-CMIP5 dataset were lower than the observations from the meteorological stations in general. After the downscaling processes, the MAE of DMAT for the whole of China was reduced to 0.67 °C and the accuracy was increased by 67.16%. The improved ratios of the MAEs were 84.48, 75.22, 68.6 and 7.2%, respectively for the Tibet plateau, the arid area, the Loess plateau, and the Sichuan Basin plus the Yunnan-Guizhou plateau.

The MAE of OMAP from the China-CMIP5 dataset was 350.52 mm for the whole of China on average. The MAEs were larger in the Tibet plateau, Loess plateau and Sichuan Basin plus Yunnan-Guizhou plateau, given values of 770.51, 656.57 and 386.03 mm, respectively. The OMAP from the China-CMIP5 dataset was higher than the observed values in general. The downscaling process reduced the MAE of DMAP to 79.12 mm and led to an improved ratio of 77.43%, when applied to the whole land mass of China. The improved ratios of the MAEs were greater than 77.43% for the Tibet plateau, arid area, the Loess plateau and northeastern China (97.09, 96.35, 91.34, 88.53 and 88.42%, respectively).

In short, the China-CMIP5 dataset had problems such that it was unable to describe climatic features on regional levels in China well and to express the variability of regional climates. The method combining HASM with geostatistics meant the China-CMIP5 dataset was able to be downscaled from 1° × 1° to 1 km × 1 km and that the accuracy

Table 2
A comparison of errors from the China-CMIP5 dataset with those from downscaled results.

Region	OTAE(°C)	DTAE(°C)	OTAE-DTAE (°C)	RT (%)	OPAE(mm)	DPAE(mm)	OPAE-DPAE(mm)	RP(%)
R_1	1.53	0.68	0.85	55.56	255.98	29.63	226.35	88.42
R_2	3.39	0.84	2.55	75.22	290.13	10.60	279.53	96.35
R_3	1.12	0.44	0.68	60.71	170.59	19.56	151.03	88.53
R_4	2.58	0.81	1.77	68.60	656.57	56.84	599.73	91.34
R_5	4.64	0.72	3.92	84.48	770.51	99.50	671.01	87.09
R_6	2.64	1.13	1.51	57.20	386.03	87.55	298.48	77.32
R_7	0.62	0.21	0.41	66.13	252.03	151.03	101	40.07
R_8	1.19	0.43	0.76	63.87	211.19	86.19	125	59.19
R_9	1.21	0.61	0.6	49.59	225.47	151.28	74.19	32.90
China	2.04	0.67	1.37	67.16	350.52	79.12	271.4	77.43

Table 3
Comparison of OMAT from CMIP5 with MAT observed at meteorological stations during the period from 1976 to 2005.

Regions	Observed MAT (°C)	OMAT from CMIP5 (°C)	Difference between OMAT and MAT at all stations on average (°C)	Proportion of stations at which MAT was overestimated (%)
R_1	5.29	4.60	−0.69	23.53
R_2	7.88	4.52	−3.36	18.18
R_3	4.58	3.92	−0.66	27.71
R_4	9.58	6.98	−2.6	9.43
R_5	3.56	−0.53	−4.09	9.80
R_6	15.65	12.77	−2.88	14.68
R_7	21.63	21.07	−0.56	40.82
R_8	13.32	12.19	−1.13	18.18
R_9	17.07	16.61	−0.46	20.49
China	11.20	9.37	−1.83	22.05

Table 4
Comparison of OMAP from CMIP5 with MAP observed at meteorological stations during the period of from 1976 to 2005.

Regions	Observed MAP (mm)	OMAP from CMIP5 (mm)	Difference between OMAP and MAP at all stations on average (mm)	Proportion of stations at which MAP was overestimated (%)
R_1	355.11	589.00	233.89	98.04
R_2	130.18	367.29	237.11	93.26
R_3	581.55	733.82	152.27	92.77
R_4	490.72	1025.90	535.18	100.00
R_5	491.34	1332.84	841.5	100.00
R_6	1085.02	1484.85	399.83	83.49
R_7	1606.41	1317.03	−289.38	22.45
R_8	670.27	844.09	173.82	96.36
R_9	1463.36	1417.00	−46.36	43.80
China	800.69	1063.78	263.09	79.92

was considerably improved because of the introduction of both ground observations and HASM.

4. Discussion and conclusions

A comparison between CMIP5 data and observations at 735 meteorological stations indicated that MAT was underestimated and MAP was overestimated in general across the whole of China. OMAT from CMIP5 was lower than observed MAT at 78% of the 735 meteorological stations, and 1.83 °C lower on average across the whole of China (Table 3, Fig. 4). OMAT at the stations where MAT was underestimated was 2.81 °C lower than observed on average, led by regions R_4, R_5, R_6 and R_2 with MATs underestimated by 2.6, 4.09, 2.88 and 3.36 °C, respectively. The meteorological stations at which OMAT was overestimated were mainly located in eastern China, accounting for 22.05% of the total meteorological stations. OMAT was 1.57 °C higher than the observed MAT at the overestimated locations on average.

MAP was overestimated at 80% of the 735 meteorological stations, while the underestimation problems appeared in the regions where MAP exceeded 1500 mm (Table 4, Fig. 5). OMAP was 263.09 mm higher on average across the whole of China. At the stations where MAP was overestimated, OMAP was 393.96 mm higher on average. OMAP was overestimated at 100%, 100%, 98%, 96%, 93%, 93% and 84% of the meteorological stations in regions R_4, R_5, R_1, R_8, R_2, R_3 and R_6, respectively. The stations where MAP was underestimated were mainly distributed in regions R_7 and R_9, accounting for 78% and 56% of the stations in the two regions respectively. The OMAP values were 449.19 and 204.54 mm lower in R_7 and R_9 on average.

A statistical analysis of China-CMIP5 data indicated that MAT exhibits spatial stationarity, while MAP exhibits spatial non-stationarity. Therefore, the trend surfaces of MAT were created by OLS and those for MAP were generated by GB. When IDW, Kriging, Spline and HASM were used to improve the residuals of the OLS trend surfaces of MAT and the GB surfaces of MAP, HASM always achieved the highest accuracy.

The validation of China-CMIP5 dataset during the period from 1976 to 2005 demonstrated that the biggest errors appeared in western China. For instance, the MAEs of MAT and MAP were respectively 4.64 °C and 770.51 mm on the Tibet plateau. On average, the MAEs of MAT and MAP were respectively 2.04 °C and 350.52 mm for the whole of China. HASM-OLS and HASM-GB considerably reduced the MAEs of MAT and MAP. The improved ratios of MAEs of MAT and MAP were

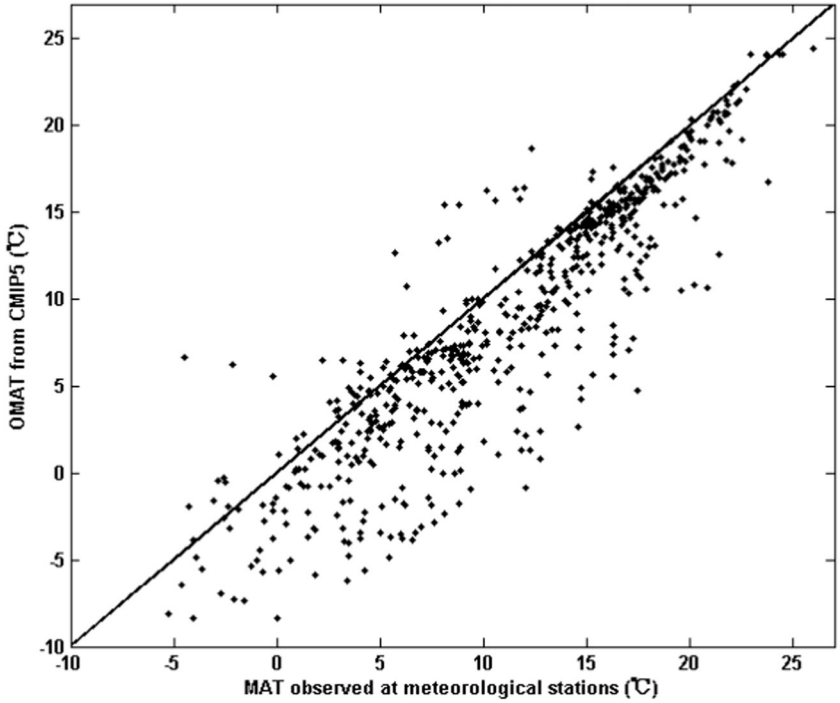

Fig. 4. Comparison between original values of mean annual temperature from CMIP5 and mean annual temperature observed at meteorological stations.

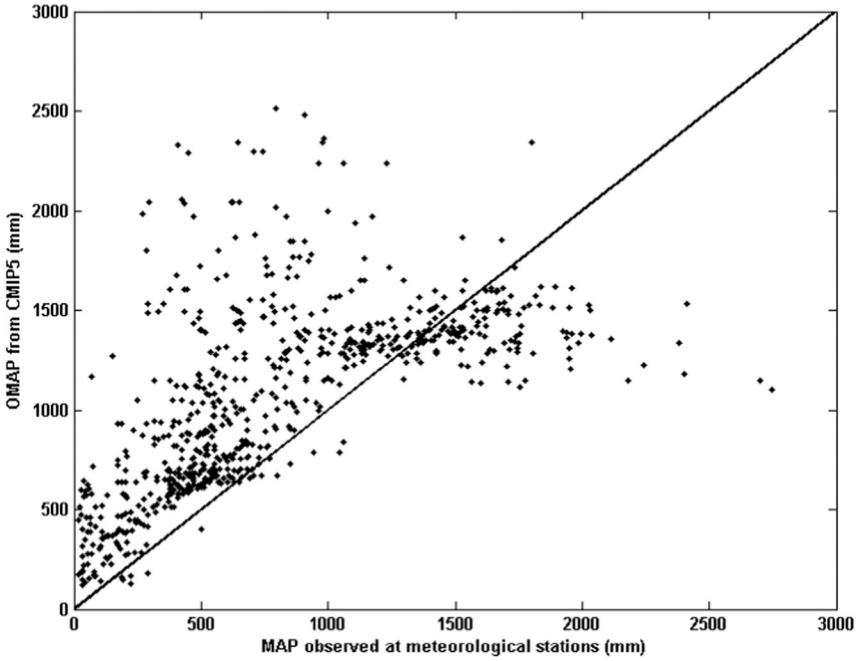

Fig. 5. Comparison between original values of mean annual precipitation from CMIP5 and mean annual precipitation observed at meteorological stations.

respectively 67.16% and 77.43% for the whole of China, and 84.48% and 97.09% for the Tibet plateau.

In terms of the China-CMIP5 dataset, the MAEs of the three scenarios of OMAT were very similar during the period 2006–2010. All of the MAEs were 2.2 °C for the whole of China on average. The regions where the MAEs exceeded 2.2 °C, included the Tibet plateau, the arid area, the Loess plateau, and the Sichuan basin plus the Yunnan-Guizhou plateau (Table 5). The MAEs of RCP2.6, RCP4.5 and RCP8.5 were respectively 5.43, 5.32 and 5.37 °C for the Tibet plateau, 4.27, 4.24 and 4.14 °C for the arid area, 2.67, 2.64 and 2.56 °C for the Loess plateau, and 2.65, 2.62 and 2.61 °C for the Sichuan basin plus the Yunan-Guizhou plateau.CMIP5 scenarios underestimated MAT mostly. Proportion of the meteorological stations, where OMAT was lower than MAT, was 88% under the scenario of RCP2.6, 88% under RCP4.5, and 87% under RCP8.5 in the whole of China. Especially, in Yangtze river basin, the proportion was more than 92% under all the three scenarios. In general, the scenario of RCP8.5 had a better performance comparing with other two scenarios.

Table 5
Mean absolute errors of mean annual temperature of RCPs during the period from 2006 to 2010 (subscripts 1, 2 and 3 of OTAE, DTAE and RT represent the scenarios of RCP2.6, RCP4.5 and RCP8.5 respectively).

Region	$OTAE_1$ (°C)	$DTAE_1$ (°C)	RT_1 (%)	$OTAE_2$ (°C)	$DTAE_2$ (°C)	RT_2 (%)	$OTAE_3$ (°C)	$DTAE_3$ (°C)	RT_3 (%)
R_1	1.45	0.67	53.58	1.46	0.68	53.67	1.42	0.67	52.64
R_2	4.27	0.86	79.92	4.24	0.85	79.84	4.14	0.86	79.31
R_3	0.90	0.46	48.26	0.92	0.46	49.67	0.89	0.46	48.01
R_4	2.67	0.98	63.26	2.64	0.98	62.89	2.56	0.98	61.78
R_5	5.43	0.69	87.26	5.32	0.70	86.93	5.37	0.69	87.09
R_6	2.65	0.85	67.97	2.62	0.85	67.59	2.61	0.85	67.51
R_7	1.13	0.29	74.49	1.07	0.29	73.02	1.13	0.29	74.40
R_8	1.58	0.32	79.91	1.55	0.32	79.55	1.52	0.32	79.21
R_9	1.48	0.40	73.14	1.48	0.40	73.14	1.45	0.40	72.58
China	2.22	0.61	72.62	2.20	0.61	72.32	2.18	0.61	72.02

After the downscaling process, all of the MAEs for the DMAT scenarios of RCP2.6, RCP4.5 and RCP8.5 were reduced to 0.61 °C for the whole land mass of China. The improved ratios of the MAEs for all of China were higher than 72%, 87% for the Tibet plateau, 79% for the arid area, 62% for the Loess plateau, and 68% for the Sichuan basin plus the Yunan-Guizhou plateau.

The statistical analysis indicated that the MAEs of OMAP under scenarios of RCP2.6, RCP4.5 and RCP8.5 were respectively 345.88, 338.18 and 340.93 mm for the whole land mass of China on average (Table 6). The Tibet plateau, Loess plateau, and the Sichuan basin plus the Yunan-Guizhou plateau had larger errors. The MAEs of the RCP2.6, RCP4.5 and RCP8.5 respectively were 758.52, 765.54 and 765.01 mm for the Tibet plateau, 583.55, 589.49 and 581.03 mm for the Loess

Table 6
Mean absolute errors of mean annual precipitation of RCPs during the period from 2006 to 2010 (subscripts 1, 2 and 3 of OPAE, DPAE and RP represent the scenarios of RCP2.6, RCP4.5 and RCP8.5 respectively).

Region	$OPAE_1$ (mm)	$DPAE_1$ (mm)	RP_1 (%)	$OPAE_2$ (mm)	$DPAE_2$ (mm)	RP_2 (%)	$OPAE_3$ (mm)	$DPAE_3$ (mm)	RP_3 (%)
R_1	284.65	13.19	95.37	263.52	12.91	95.10	271.36	13.82	94.91
R_2	229.66	20.79	90.95	228.15	20.43	91.05	220.40	20.46	90.72
R_3	211.68	37.99	82.05	197.19	37.77	80.84	209.16	38.07	81.80
R_4	583.55	67.74	88.39	589.49	66.39	88.74	581.03	68.01	88.29
R_5	758.52	72.89	90.39	765.54	71.87	90.61	765.01	72.55	90.52
R_6	400.94	59.90	85.06	392.47	56.39	85.63	402.05	56.55	85.93
R_7	308.54	92.25	70.10	309.56	91.15	70.55	302.86	93.34	69.18
R_8	252.95	70.60	72.09	230.29	70.66	69.32	246.40	70.89	71.23
R_9	211.93	165.27	22.02	204.29	163.34	20.04	202.04	163.97	18.84
China	345.88	71.01	79.47	338.18	70.21	79.24	340.923	70.85	79.22

plateau, and 400.94, 392.47 and 402.05 mm for the Sichuan basin plus the Yunan-Guizhou plateau. At 80% of the meteorological stations, precipitation was overestimated by all the three scenarios of CMIP5. Especially, in the area covered by Tibet plateau, Loess plateau and Inner Mongolia plateau, all the three scenarios were bigger than actual precipitation at all the meteorological stations. However, the actual precipitation was smaller than all the scenarios at almost all stations where MAP was bigger than 1500 mm. The scenario of RCP4.5 performed better comparatively.

The downscaling process made the DMAP 70% more accurate than OMAP for the whole of China on average. The improved ratios of MAEs were more than 90% in northeast Inner Mongolia, in the arid area, and the Tibet plateau. The MAEs of the three scenarios were decreased to 13.19, 12.91 and 13.82 mm in northeast Inner Mongolia, to 20.79, 20.43 and 20.46 mm in the arid area, and to 72.89, 71.87 and 72.55 mm for the Tibet plateau. However, the MAEs of the DMAP for the three scenarios were still as high as 165.27, 163.34 and 163.97 mm respectively in the middle and lower reaches of the Yangtze River.

Acknowledgments

This work is supported by the National Natural Science Foundation of China (91325204), by the National High-tech R&D Program of the Ministry of Science and Technology of the People's Republic of China (2013AA122003), and by National Basic Research Priorities Program of Ministry of Science and Technology of the People's Republic of China (2010CB950904). We thank the modeling groups for providing their data for analysis, the Program for Climate Model Diagnosis and Intercomparison (PCMDI) and the World Climate Research Program's (WCRP's) Coupled Model Inter-comparison Project for organizing the model data analysis activity, collecting and archiving the model output. The data has been collected, analyzed, and are provided by National Climate Center of China.

References

Anthes, R.A., 1983. Regional models of the atmosphere in middle latitudes. Mon. Weather Rev. 111, 1306–1335.
Box, G.E.P., Cox, D.R., 1964. An analysis of transformations. J. Roy. Stat. Soc. B 26 (2), 211–252.
Charles, S.P., Bates, B.C., Whetton, P.H., Hughes, J.P., 1999. Validation of downscaling models for changed climate conditions: case study of southwestern Australia. Clim. Res. 12, 1–14.
Chu, J.T., Xia, J., Xu, C.Y., Singh, V.P., 2010. Statistical downscaling of daily mean temperature, pan evaporation and precipitation for climate change scenarios in Haihe River, China. Theor. Appl. Climatol. 99, 149–161.
Ciret, C., Sellers, A.H., 1998. Sensitivity of ecosystem models to the spatial resolution of the NCAR Community Climate ModelCCM2. Clim. Dyn. 14, 409–429.
Dibike, Y., Gachon, P., St-Hilaire, A., Ouarda, T.B.M.J., Nguyen, V.T.V., 2008. Uncertainty analysis of statistically downscaled temperature and precipitation regimes in northern Canada. Theor. Appl. Climatol. 91, 149–170.
Dickinson, R.E., Errico, R.M., Giorgi, F., Bates, G.T., 1989. A regional climate model for the western U.S. Clim. Chang. 15, 383–422.
Gachon, P., Dibike, Y., 2007. Temperature change signals in northern Canada: convergence of statistical downscaling results using two driving GCMs. Int. J. Climatol. 27, 1623–1641.
Giorgi, F., 1990. Simulation of regional climate using a limited area model nested in a general circulation model. J. Clim. 3, 941–963.
Grotch, S.L., MacCracken, M.C., 1991. The use of general circulation models to predict regional climate change. J. Clim. 4, 286–303.
Harding, K.J., Snyder, P.K., Liess, S., 2013. Use of dynamical downscaling to improve the simulation of central U.S. warm season precipitation in CMIP5 models. J. Geophys. Res. Atmos. 118, 12522–12536.
Haylock, M.R., Cawley, G.C., Harpham, C., Wilby, R.L., Goodess, C.M., 2006. Downscaling heavy precipitation over the United Kingdom: a comparison of dynamical and statistical methods and their future scenarios. Int. J. Climatol. 26, 1397–1415.
Hewitson, B.C., Crane, R.G., 1996. Climate downscaling: techniques and application. Clim. Res. 7, 85–95.
Huang, D.Q., Zhu, J., Zhang, Y.C., Huang, A.N., 2013. Uncertainties on the simulated summer precipitation over eastern China from the CMIP5 models. J. Geophys. Res. Atmos. 118, 9035–9047.
Jia, S.F., Zhu, W.B., Lǔ, A.F., Yan, T.T., 2011. A statistical spatial downscaling algorithm of TRMM precipitation based on NDVI and DEM in the Qaidam Basin of China. Remote Sens. Environ. 115, 3069–3079.
Jones, P.D., Murphy, J.M., Noguer, M., 1995. Simulation of climate changeover Europe using a nested regional-climate model, I: assessment of control climate, including sensitivity to location of lateral boundaries. Q. J. R. Meteorol. Soc. 121, 1413–1449.
Khalili, M., Van Nguyen, V.H., Gachon, P., 2013. A statistical approach to multi-site multivariate downscaling of daily extreme temperature series. Int. J. Climatol. 33, 15–32.
Laprise, R., 2008. Regional climate modelling. J. Comput. Phys. 227, 3641–3666.
Li, Z., Zheng, F.L., Liu, W.Z., Jiang, D.J., 2012. Spatially downscaling GCMs outputs to project changes in extreme precipitation and temperature events on the Loess Plateau of China during the 21st century. Glob. Planet. Chang. 82-83, 65–73.
Liu, Y., Fan, K., 2013. A new statistical downscaling model for autumn precipitation in China. Int. J. Climatol. 33 (6), 1321–1336.
Liu, L.L., Liu, Z.F., Ren, X.Y., Fischer, T., Xu, Y., 2011a. Hydrological impacts of climate change in the Yellow River basin for the 21st century using hydrological model and statistical downscaling model. Quat. Int. 244, 211–220.
Liu, Z.F., Xu, Z.X., Charles, S.P., Fu, G.B., Liu, L., 2011b. Evaluation of two statistical downscaling models for daily precipitation over an arid basin in China. Int. J. Climatol. 31, 2006–2020.
Pielke Sr., R.A., Wilby, R.L., 2012. Regional climate downscaling: what's the point? Eos 93, 52–53.
Prudhomme, C., Davies, H., 2009. Assessing uncertainties in climate change impact analyses on the river flow regimes in the UK, part 1: baseline climate. Clim. Chang. 93, 177–195.
Raisanen, J., 2007. How reliable are climate models? Tellus A 59, 2–29.
Tselioudis, G., Douvis, C., Zerefos, C., 2012. Does dynamical downscaling introduce novel information in climate model simulations of precipitation change over a complex topography region? Int. J. Climatol. 32, 1572–1578.
von Storch, H., Zorita, E., Cubash, U., 1993. Downscaling of global climate change estimates to regional scales: an application to Iberian rainfall in wintertime. J. Clim. 6, 1161–1671.
Walsh, K.J.E., McGregor, J.L., 1997. An assessment of simulations of climate variability over Australia with a limited area model. Int. J. Climatol. 17, 201–223.
Wilby, R.L., Dawson, C.W., Barrow, E.M., 2002. SDSM-a decision support tool for the assessment of regional climate change impact. Environ. Model. Softw. 17, 147–159.
Xu, C.Y., 1999. From GCMs to river flow: a review of downscaling methods and hydrologic modelling approaches. Prog. Phys. Geogr. 23, 229–249.
Xue, Y.K., Vasic, R., Janjic, Z., Mesinger, F., Mitchell, K.E., 2007. Assessment of dynamic downscaling of the continental U.S. regional climate using the Eta/SSiB regional climate model. J. Clim. 20, 4172–4193.
Yang, T., Li, H.H., Wang, W.G., Xu, C.Y., Yu, Z.B., 2012. Statistical downscaling of extreme daily precipitation, evaporation, and temperature and construction of future scenarios. Hydrol. Process. 26, 3510–3523.
Yuan, X., Liang, X.Z., Wood, E.F., 2012. WRF ensemble downscaling seasonal forecasts of China winter precipitation during 1982–2008. Clim. Dyn. 39, 2041–2058.
Yue, T.X., 2011. Surface Modelling: High Accuracy and High Speed Methods. CRC Press, New York.
Yue, T.X., Zhao, N., Ramsey, R.D., Wang, C.L., Fan, Z.M., Chen, C.F., Lu, Y.M., Li, B.L., 2013a. Climate change trend in China, with improved accuracy. Clim. Chang. 120, 137–151.
Yue, T.X., Zhao, N., Yang, H., Song, Y.J., Du, Z.P., Fan, Z.M., Song, D.J., 2013b. The multi-grid method of high accuracy surface modelling and its validation. Trans. GIS 17, 943–952.
Zhou, L.S., Sun, H., Shen, Y.Q., Deng, J.Z., Shi, Y.L., 1981. Comprehensive Agricultural Planning of China. China Agricultural Press, Beijing in Chinese.
Zorita, E., von Storch, H., 1999. The analog method as a simple statistical downscaling technique: comparison with more complicated methods. J. Clim. 12, 2474–2489.